Electronic Supplementary Material (ESI) for Nanoscale Advances.

Supporting Information

For

Scalable synthesis of gyroid-inspired freestanding three-dimensional graphene architectures

Adrian E. Garcia,[a] Chen Santillan Wang,[a] Robert N. Sanderson,[b] Kyle McDevitt,[a] Yunfei Zhang,[c] Lorenzo Valdevit,[a,⊥] Daniel Mumm,[a] Ali Mohraz,[d] and Regina Ragan[a,*]

[a.]Department of Chemical Engineering and Material Science, University of California, Irvine, Irvine, CA 92697-2585, [b.]Department of Physics and Astronomy, University of California, Irvine, Irvine, CA 92697-4575, [c.]Department of Mechanical and Aerospace Engineering, University of California, Irvine, Irvine, CA 92697-2700, [d.]Department of Chemical and Biochemical Engineering, University of California, Irvine, Irvine, CA 92697-2580

[*] corresponding author

This file includes:

Supplementary materials of scanning electron microscopy images, Raman Spectroscopy and X-ray photoelectron spectroscopy

Supplementary figures S1-S5

1. Scanning Electron Microscopy

Scanning electron microscopy (SEM) images of bi-Ni and bi-Ni-3DG sample cross-sections are shown in Fig. S1. The bi-Ni sample shown in Fig. S1a underwent thermal treatment for pyrolysis of the polymer template at 500 °C and then reduction of NiO at 450 °C. The bi-Ni-3DG in Fig. S1b was fabricated via chemical vapor deposition (CVD) using methane as the carbon precursor at 900 °C as described in Fig. 2c of the main text. The sample was cut from the low right side perpendicular to the bi-Ni long axis.

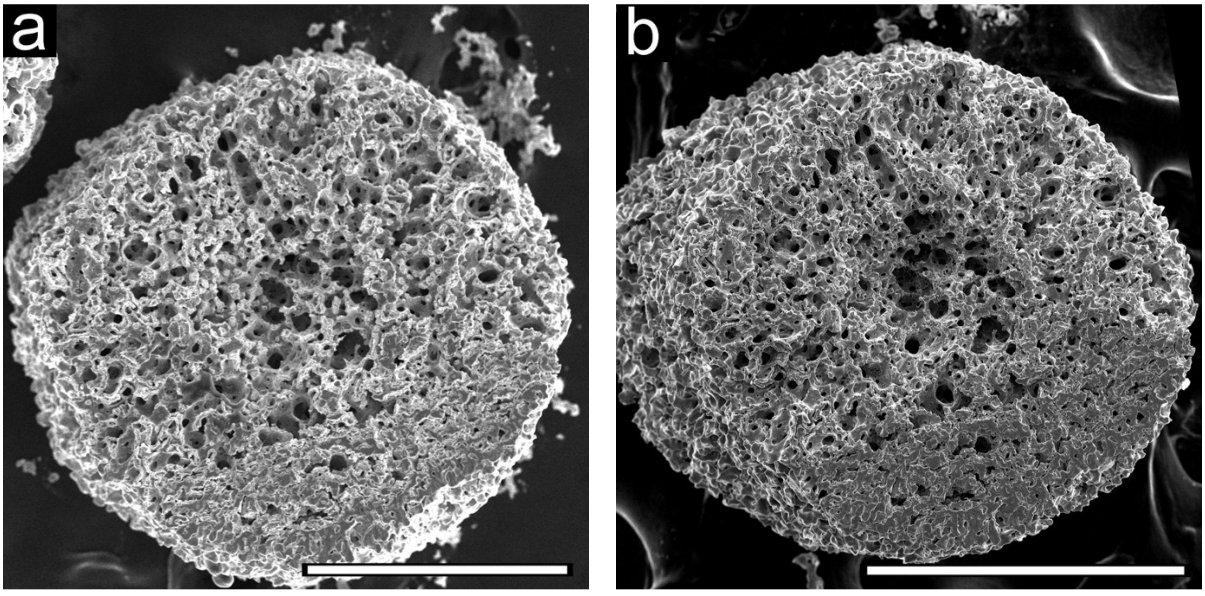

Figure S 1. bi-Ni (a) and bi-Ni-3DG (b) cross section. The scale bar is 400 µm for both images.

2. X-ray photoelectron spectroscopy

Fig. S2 shows X-ray photoelectron spectroscopy (XPS) spectra acquired from a bijel templated sample. In Fig. S2 (a), an XPS survey spectrum of bi-3DG from 0 eV to 1200 eV is depicted. From this data, the C/O ratio is determined to be approximately 17:1; Higher energy resolution XPS data of the C 1s peaks for bi-Ni, bi-Ni-3DG, and bi-3DG are presented in Fig. S2

(b-d). Deconvolution of the C1s spectrum of bi-Ni in Fig. S2 (b) show a primary C-C peak centered at 285 eV with a large secondary C-O peak at 286.2 eV and a similarly sized C=O peak at 289.4 eV. All peaks here are modeled with a Voigt line shape. The presence of C-O and C=O bonds in bi-Ni are attributed to originate from trace amounts of polymer residue. After CVD, XPS is performed on bi-Ni-3DG with C 1s spectral data shown in Fig. S2 (c); the primary C 1s peak shifts to 284.3 eV and displays an asymmetric line shape with a tail extending into higher binding energy, a clear indication of sp2 C=C bonding. This observation coupled with the metal/semi-metal behavior of sp2 carbon suggests that a Doniach-Sunjic[1] (DS) line shape is appropriate to model the C=C contribution. The presence of a Gaussian shoulder at 284.7 eV is attributed to instrumental broadening.[2] An asymmetry parameter of 0.055 is used for DS, which agrees with previous work.[2] A Voigt line shape is used to model the smaller C-O contribution at 286.1 eV, which are attributed to the phenol groups.[3] The complex plasmon spectra of graphitic materials results in satellites,[4] which are fitted here with a Gaussian line shape at 290.4 eV.

C 1s peak fitting is a complex challenge with the peaks of some components overlapping in origin.[5] Previous literature has referred to a contribution near 284.9 eV as "carbon defects"[6,7] and slightly higher BE (285 – 285.6 eV) contributions as sp3 carbon,[8] of which, the latter is not observed in the XPS spectra. In regards to carbon defects, Raman spectroscopy would highlight defects in the material with a "D" peak near 1350 cm^{-1}. As discussed and shown in Fig. 4a and 6a, no such peaks are found. Additionally, Raman spectra would indicate sp3 carbon with a broad "G" peak[9] centered near 1580 cm^{-1}, however all G peaks in this dataset are well fit with a single Lorentzian. Thus attributing the 284.7 eV peak to instrumental broadening is consistent with both Raman data discussed below and prior analysis.[10] Fig. S2 (d) shows that bi-3DG is

similar to bi-Ni-3DG. The sp2 contribution, C=C, contributes 92% of peak intensity and C-O contributes the remainder.

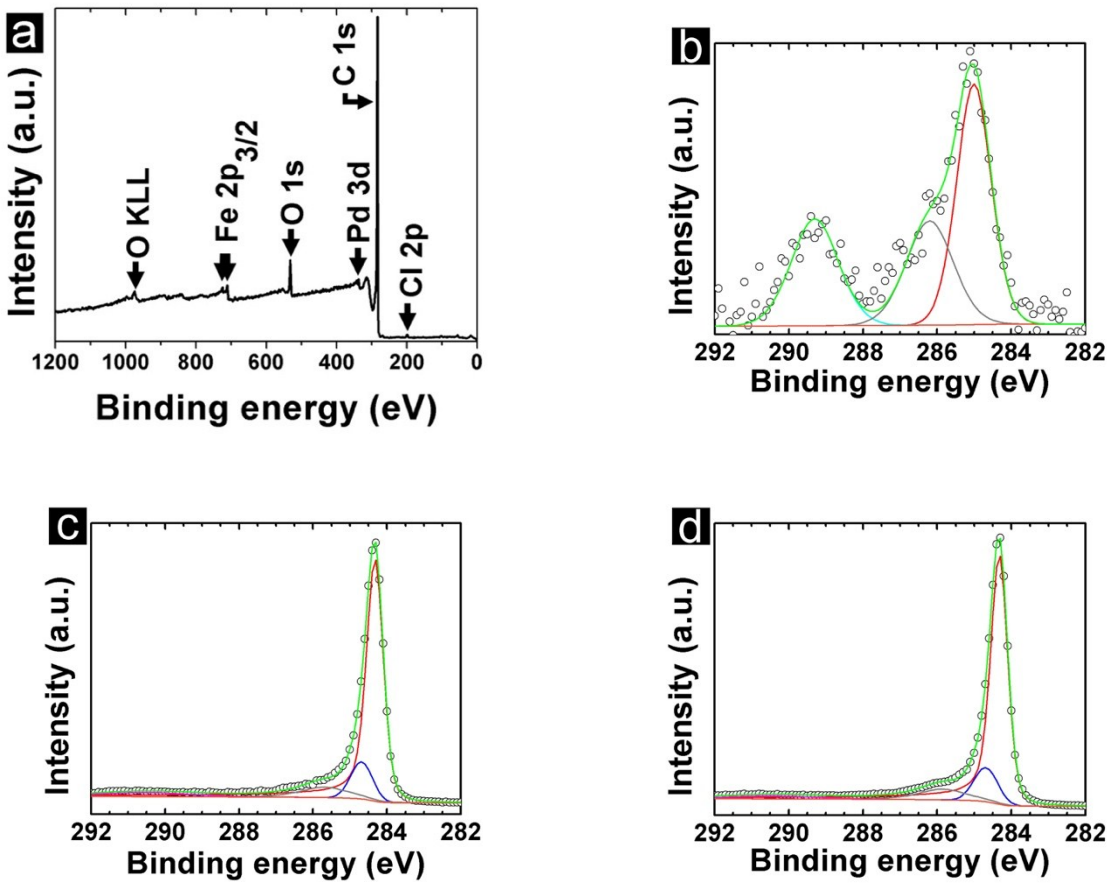

Figure S 2.(a) Survey XPS data for bi-3DG. High resolution data of C 1s from (b) bi-Ni, (c) bi-Ni-3DG, and (d) bi-3DG.

3. Raman Spectroscopy

Raman spectra were acquired over at least 30 distinct points on each sample with 50 micron spacing between measurements. Histograms for the measured I_{2D} full-width at half maximum (FWHM) and the I_{2D}/I_G ratio are shown in Fig. S3. Changes in both the I_{2D} FWHM and the I_{2D}/I_G

ratio are used to further understand the interlayer stacking structure. The most commonly observed layer stacking in multilayer graphene (MLG) is either AB (Bernal) or twisted (also known as rotationally-faulted or turbostratic)[11] and the two can be differentiated by examining Raman spectral features.[12] Turbostratic graphene arises due to rotational disorder which decreases interlayer coupling.[13] Due to the decreased interactions, carrier mobility in turbostratic graphene may be comparable to that in single layer graphene (SLG).[14,15] Specifically, turbostratic stacking in multilayer graphene may be identified by any of the following cases: I) abnormally enhanced I_G intensity,[12,16] II) I_{2D} / I_G ratios approaching those observed on SLG ,[17] III) combination Raman modes,[14] IV) blueshifted I_{2D} peak position with FWHM typically less than 55 cm^{-1}.[12,18]

Analysis of bi-Ni-3DG Raman data displays a broad range of values for the I_{2D} FWHM and I_{2D} / I_G as observed in the histograms of Fig. S3 (a-b). Spatial variations in the stacking behavior of CVD graphene films produced on Ni substrates are expected,[19] with previous work reporting the presence of Bernal stacking and turbostratic layers.[20,21] In the histogram of Fig. S3 (a), the I_{2D} FWHM values range from 24 cm^{-1} to 85 cm^{-1} with an average probability density value of 54 cm^{-1} ± 13 cm^{-1}. The average value of I_{2D} FWHM after Ni etching is approximately the same, 55 cm^{-1} ± 11 cm^{-1}, for bi-3DG. Values of I_{2D} FWHM less than 55 cm^{-1} has been attributed to rotation angles greater than 5 degrees. This is further corroborated by an average I_{2D} peak position of 2698 $\pm$ 8 cm^{-1}. The distribution of FWHM values suggests a mixture of turbostratic stacking (case IV) along with Bernal stacking, where FWHM values are typically greater than 60 cm^{-1} in Bernal stacked multilayer graphene. The histogram of I_{2D} / I_G, shown in Fig. S3 (b) exhibits a distribution maximum centered near 0.8 with an average value of 1.4 $\pm$ 1.2. An outlier spectrum is found to exhibit I_{2D} / I_G of 7.4 and I_{2D} FWHM of 24 cm^{-1}, features associated with turbostratic

graphene (case II).[17] The inclusion of spectra in the histogram with I_{2D} / I_G ratios greater than 1 further indicates the presence of turbostratic graphene.

Fig. S3 (c-d) shows histograms of I_{2D} FWHM and I_{2D} / I_G of a sample after etching the Ni scaffold (bi-3DG). The I_{2D} FWHM histogram in Fig. S3 (c) transitions to a more clearly separated bimodal distribution with the primary maxima at 60 cm^{-1}, secondary maxima at 35 cm^{-1}, and a range of 30 cm^{-1} to 68 cm^{-1}. This indicates a higher degree of spatial uniformity in graphene stacking compared to the broader distribution in bi-Ni-3DG. Fig. S3 (d) shows the bi-3DG histogram of I_{2D} / I_G with distribution primarily centered around 0.5 with an average of 0.9 + 0.6. The process of etching the Ni scaffold seems to promote graphene layers to relax and collapse onto one another.

Fig. S3 (e-f) shows histograms of Raman data analysis, I_{2D} FWHM and I_{2D}/I_G, of bi-2-3DG which were made from a bi-Ni-2 scaffold (annealed at 900 °C in forming gas before CVD growth). Here, the I_{2D} FWHM distribution in Fig. S3 (e) is still bimodal but the maxima is near 40 cm^{-1} with a range of 31 cm^{-1} to 74 cm^{-1}, signaling a shift towards FWHM values associated with turbostratic graphene as compared to Fig. S3 (c). Fig. S3 (f) shows that these narrow FWHMs are corroborated by an increase in the number of 2D/G ratios above 1.0 with an average ratio of 1.0 $\pm$ 0.5. 20% of the spectra exhibit combination Raman modes (case III) in this dataset with peak positions corresponding to turbostratic stacking.[14] The noticeable increase in narrow FWHM and I_{2D}/I_G ratios greater than 1.0 from Fig. S3 (c-d) to Fig. S3 (e-f) demonstrates the ability to tune the material towards fewer layers and turbostratic stacking using CVD and thermal processing of bijel templates.

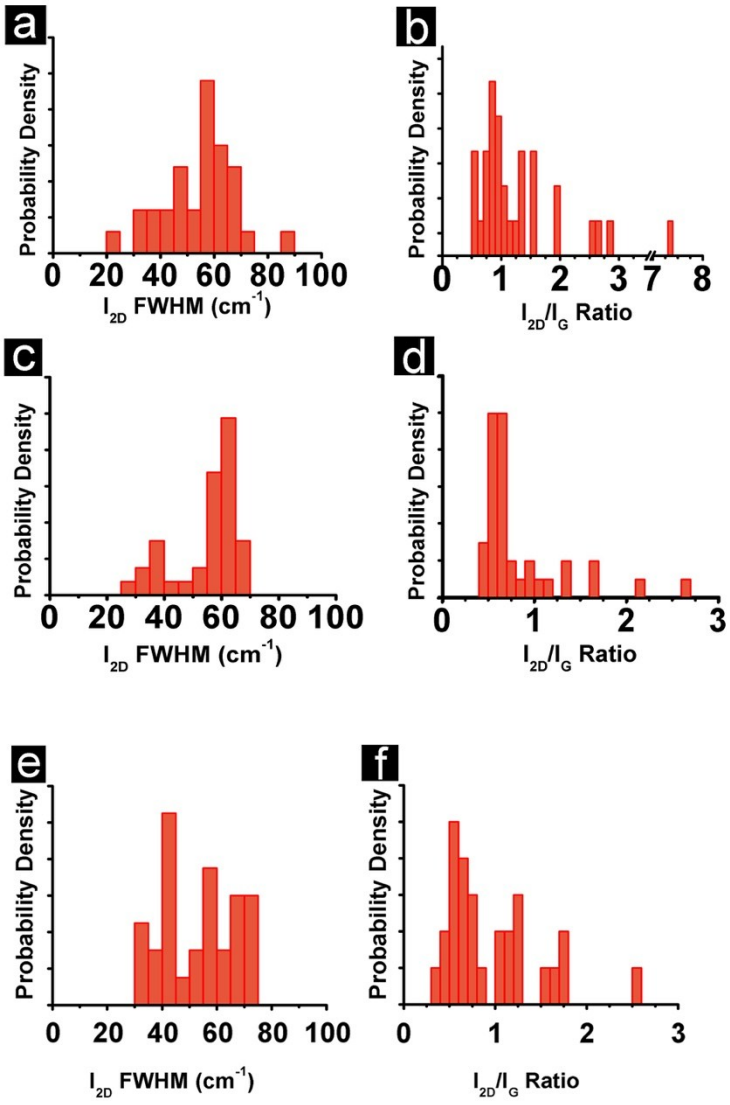

Figure S 3. Probability density histograms showing results of Raman spectrum analysis. The measured values for the 2D peak FWHM and the intensity ratio I_{2D}/I_G (bin sizes of 5 and 0.2, respectively) are shown for (a and b) bi-Ni-3DG, (c and d) bi-3DG, and (e and f) bi-2-3DG. Standard deviations of data sets a, b, c, d, e, and f are 13 cm^{-1}, 1.2, 10.9 cm^{-1}, 0.6, 13 cm^{-1} and 0.5, respectively.

Fig. S4 shows analysis of Raman data from the 2DG analogue. The FWHM value observed with the highest probability is approximately 70 cm^{-1}. The 2D/G ratio observed with highest probability is 0.5 with an average of 1.2 $\pm$ 1.3. There are regions where the FWHM has the signature of

turbostratic graphene and other regions where the FWHM approaches higher values expected for Bernal layer stacking in MLG. The similarity between bi-Ni-3DG in Fig. S3 (a-b) and the 2DG analogue in Fig. S4 (a-b) indicates the 2D system contains representative regions on the sample for the scanning tunneling microscopy analysis presented in Fig. 5.

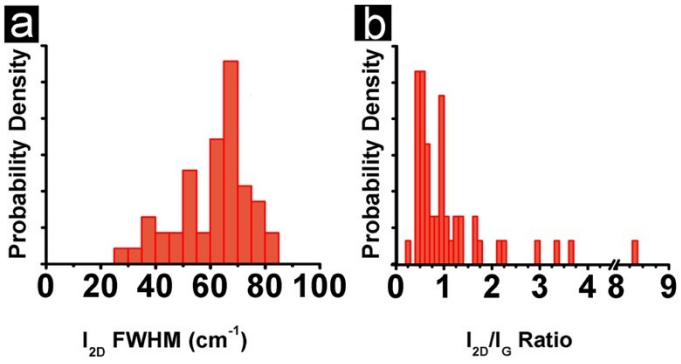

Figure S 4. The measured values for the 2D peak FWHM (a) and the intensity ratio I_{2D}/I_G (b) for 2DG. Standard deviations of data sets a and b are 13.2 cm^{-1} and 1.3 respectively.

Higher magnification SEM images of cross sections of (a) bi-Ni and (b) bi-Ni-3DG samples are shown in Fig. S5. Examination of the pore in the center of Fig. S5 (a) shows small voids in between concentric rings of Ni. Fig. S5 (b) shows that after CVD growth, the voids are no longer visible, indicating that the Ni films have sintered.

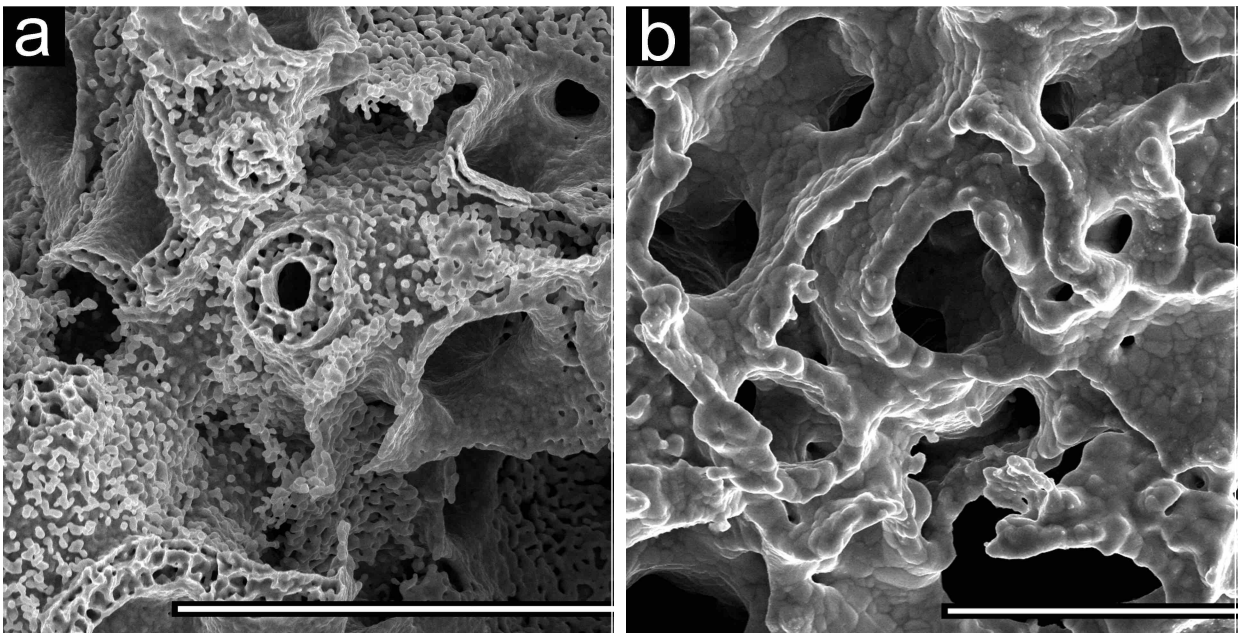

Figure S 5. (a) SEM image of bi-Ni cross section after pyrolysis of PEGDA where voids are observed in between concentric rings of Ni films. (b) SEM image of bi-Ni-3DG cross section indicates that Ni sinters during the CVD growth process since voids are no longer observed. Scale bars are 30 μm.

Supplementary Notes and References:

1. S. Doniach and M. Sunjic, Many-electron singularity in X-ray photoemission and X-ray line spectra from metals, *J. Phys. C Solid State Phys.*, 1970, **3**, 285.
2. T. Susi, T. Pichler and P. Ayala, X-ray photoelectron spectroscopy of graphitic carbon nanomaterials doped with heteroatoms, *Beilstein J. Nanotechnol.*, 2015, **6**, 177–192.
3. H. P. Boehm, Surface oxides on carbon and their analysis: a critical assessment, *Carbon*, 2002, **40**, 145–149.
4. M. Guzzo, J. J. Kas, L. Sponza, C. Giorgetti, F. Sottile, D. Pierucci, M. G. Silly, F. Sirotti, J. J. Rehr and L. Reining, Multiple satellites in materials with complex plasmon spectra: From graphite to graphene, *Phys. Rev. B*, 2014, **89**, 085425.
5. G. Speranza, L. Minati and M. Anderle, The C 1 s core line in irradiated graphite, *J. Appl. Phys.*, 2007, **102**, 043504.
6. N. G. Shang, P. Papakonstantinou, M. McMullan, M. Chu, A. Stamboulis, A. Potenza, S. S. Dhesi and H. Marchetto, Catalyst-free efficient growth, orientation and biosensing properties of multilayer graphene nanoflake films with sharp edge planes, *Adv. Funct. Mater.*, 2008, **18**, 3506–3514.
7. W. Zhang, J. Cui, C. Tao, Y. Wu, Z. Li, L. Ma, Y. Wen and G. Li, A strategy for producing pure single-layer graphene sheets based on a confined self-assembly approach, *Angew. Chem.*, 2009, **121**, 5978–5982.

8. A. Siokou, F. Ravani, S. Karakalos, O. Frank, M. Kalbac and C. Galiotis, Surface refinement and electronic properties of graphene layers grown on copper substrate: an XPS, UPS and EELS study, *Appl. Surf. Sci.*, 2011, **257**, 9785–9790.
9. J. Schwan, S. Ulrich, V. Batori, H. Ehrhardt and S. R. P. Silva, Raman spectroscopy on amorphous carbon films, *J. Appl. Phys.*, 1996, **80**, 440–447.
10. A. C. Brieva, C. Jäger, F. Huisken, L. Šiller and Y. V. Butenko, A sensible route to covalent functionalization of carbon nanoparticles with aromatic compounds, *Carbon*, 2009, **47**, 2812–2820.
11. A. Bianco, H.-M. Cheng, T. Enoki, Y. Gogotsi, R. H. Hurt, N. Koratkar, T. Kyotani, M. Monthioux, C. R. Park and J. M. Tascon, *All in the graphene family–a recommended nomenclature for two-dimensional carbon materials*, Elsevier, 2013.
12. K. Kim, S. Coh, L. Z. Tan, W. Regan, J. M. Yuk, E. Chatterjee, M. F. Crommie, M. L. Cohen, S. G. Louie and A. Zettl, Raman spectroscopy study of rotated double-layer graphene: misorientation-angle dependence of electronic structure, *Phys. Rev. Lett.*, 2012, **108**, 246103.
13. A. C. Ferrari, Raman spectroscopy of graphene and graphite: Disorder, electron–phonon coupling, doping and nonadiabatic effects, *Solid State Commun.*, 2007, **143**, 47–57.
14. J. A. Garlow, L. K. Barrett, L. Wu, K. Kisslinger, Y. Zhu and J. F. Pulecio, Large-area growth of turbostratic graphene on Ni (111) via physical vapor deposition, *Sci. Rep.*, 2016, **6**, 19804.
15. N. Richter, Y. R. Hernandez, S. Schweitzer, J.-S. Kim, A. K. Patra, J. Englert, I. Lieberwirth, A. Liscio, V. Palermo and X. Feng, Robust two-dimensional electronic properties in three-dimensional microstructures of rotationally stacked turbostratic graphene, *Phys. Rev. Appl.*, 2017, **7**, 024022.
16. J. T. Robinson, J. Culbertson, M. Berg and T. Ohta, Work function variations in twisted graphene layers, *Sci. Rep.*, 2018, **8**, 2006.
17. U. Mogera, R. Dhanya, R. Pujar, C. Narayana and G. U. Kulkarni, Highly decoupled graphene multilayers: turbostraticity at its Best, *J. Phys. Chem. Lett.*, 2015, **6**, 4437–4443.
18. A. C. Ferrari, J. C. Meyer, V. Scardaci, C. Casiraghi, M. Lazzeri, F. Mauri, S. Piscanec, D. Jiang, K. S. Novoselov, S. Roth and A. K. Geim, Raman Spectrum of Graphene and Graphene Layers, *Phys. Rev. Lett.*, 2006, **97**, 187401.
19. A. Dahal and M. Batzill, Graphene–nickel interfaces: a review, *Nanoscale*, 2014, **6**, 2548–2562.
20. A. Reina, X. Jia, J. Ho, D. Nezich, H. Son, V. Bulovic, M. S. Dresselhaus and J. Kong, Large Area, Few-Layer Graphene Films on Arbitrary Substrates by Chemical Vapor Deposition, *Nano Lett.*, 2009, **9**, 30–35.
21. Z. Chen, W. Ren, L. Gao, B. Liu, S. Pei and H.-M. Cheng, Three-dimensional flexible and conductive interconnected graphene networks grown by chemical vapour deposition, *Nat. Mater.*, 2011, **10**, 424.